RSC Advances

PAPER

View Article Online
View Journal | View Issue

Cite this: *RSC Adv.*, 2024, **14**, 7006

A eutectogels-catalyzed one-pot multi-component reaction: access to pyridine and chromene derivatives†

Phat Ngoc Nguyen, [ab] Linh Ho Thuy Nguyen, [bc] Tan Le Hoang Doan, [bc] Phuong Hoang Tran [ab] and Hai Truong Nguyen *[ab]

Received 5th January 2024
Accepted 23rd February 2024

DOI: 10.1039/d4ra00123k

rsc.li/rsc-advances

The demand for a wide array of functional chemicals and materials has experienced a significant surge in tandem with the advancement of civilization. Regrettably, a number of perilous solvents are employed in chemical laboratories and industrial settings, posing significant risks to the well-being of researchers and contributing to environmental degradation through pollution. Eutectogels, which are based on the eutectic concept, may be synthesized by self-assembling or self-polymerization of various components when put under UV irradiation (254 nm). A novel copolymeric deep eutectic solvent (DES) was successfully synthesized, comprising choline chloride (HBA) as the hydrogen bond acceptor, acetamide (HBD) as the hydrogen bond donor, tetraethyl orthosilicate (TEOS), and formic acid. In this study, we present the preparation of four-component ETGs for synthesizing pyridine and chromene derivatives as a reusable catalyst through a multi-component pathway without solvents. The procedure of synthesizing these heterocyclic compounds is free of using toxic solvents and it could be categorized as a green method.

Introduction

The need for numerous functional chemicals and materials has increased dramatically as civilization has progressed.[1] The categories of synthesized products range from nanoscale to macroscale.[2] The majority of synthetic chemical transformation processes include the use of various organic solvents.[1] Unfortunately, several of these hazardous solvents get used in chemical laboratories and industry, and have been identified as a major threat to researcher health, as well as environmental harm caused by pollution. Therefore, applications of solvent-free reactions in organic chemistry synthesis can provide a new opportunity to tackle the issue of using environmentally hazardous solvents.[3,4]

A quest for alternatives to nonrenewable fossil resources has been motivated by environmental worries and energy security. Sustainable solvents are required to possess a range of distinct environmentally friendly, well-being, and compliance characteristics that distinguish them from conventional solvent-based solutions.[5] Ionic solutions, adjustable solvents, and deep eutectic solvents (DESs) have garnered significant attention and have been widely investigated in this field of research.[6,7] DESs are characterized as mixtures consisting of more than one component that are immiscible but have the ability to form a homogeneous phase of liquid with a freezing temperature lower compared to that of each component individually.[8–11] Eutectogels, which are based on the eutectic concept, may be synthesized by self-assembling or self-polymerization of various components.[2,12–14] Joos *et al.* introduced the name "eutectogel" when they put forward DES-silica composite materials as a prospective material for solid composite electrolytes (SCEs).[15] The composites that were synthesized consisted of a silica framework with a DES embedded inside. These composites were given the name eutectogels (ETGs) and were classified as a novel kind of solid-state electrolytes (SCEs). Subsequently, several composites, including DES, were denoted as eutectogels by subsequent research groups.[16] In a scientific work produced by the research team Wang *et al.*, the authors have divided the DES-ETGs into three unique groups. There are three types of polymer gels that include the use of deep eutectic solvents (DESs) including eutectogels-S, eutectogels-P, and supramolecular eutectogels. In eutectogels-S, DESs are used as solvents inside the polymer gel. In eutectogels-P, DESs serve as both solvents and monomers during polymerization reactions. Lastly, supramolecular eutectogels are supramolecular gels where DESs operate as solvents.[12,16]

Due to its biological effects, pyridine (and its derivatives) is one of the most significant nitrogen-containing heterocyclic aromatic chemicals.[17–20] In recent times, a variety of techniques have been employed to create pyridine structures due to their

[a]*Department of Organic Chemistry, Faculty of Chemistry, University of Science, Ho Chi Minh City, 700000, Vietnam. E-mail: ngthai@hcmus.edu.vn*

[b]*Vietnam National University, Ho Chi Minh City, 700000, Vietnam*

[c]*Center for Innovative Materials and Architectures, Vietnam National University, Ho Chi Minh City, 721337, Vietnam*

† Electronic supplementary information (ESI) available. See DOI: https://doi.org/10.1039/d4ra00123k

significant applications in fields such as cyanine dyes,[21] photovoltaic cells,[22] and particularly the pharmaceutical industry. These applications encompass a wide range of therapeutic areas, including antimalarial, anti-bacterial, anti-fungal, anti-tubercular, anti-tumor, anti-cancer, anti-HIV, anti-protozoal, anti-inflammatory, anti-oxidant, and anti-hypertensive activities.[23–28] In recent years, numerous techniques have been devised for the synthesis of pyridine derivatives. In 2013, Zeba N. Siddiqui *et al.* described a method for synthesizing pyranyl pyridine derivatives by the use of ß-enaminones and ZnO nanoparticles (Scheme 1a).[29] In 2014, Ghasemzadeh *et al.* introduced a method for synthesizing polyfunctionalized dihydropyridines using AgI nanoparticles as a highly efficient catalyst through one-pot synthetic pathway (Scheme 1b).[30]

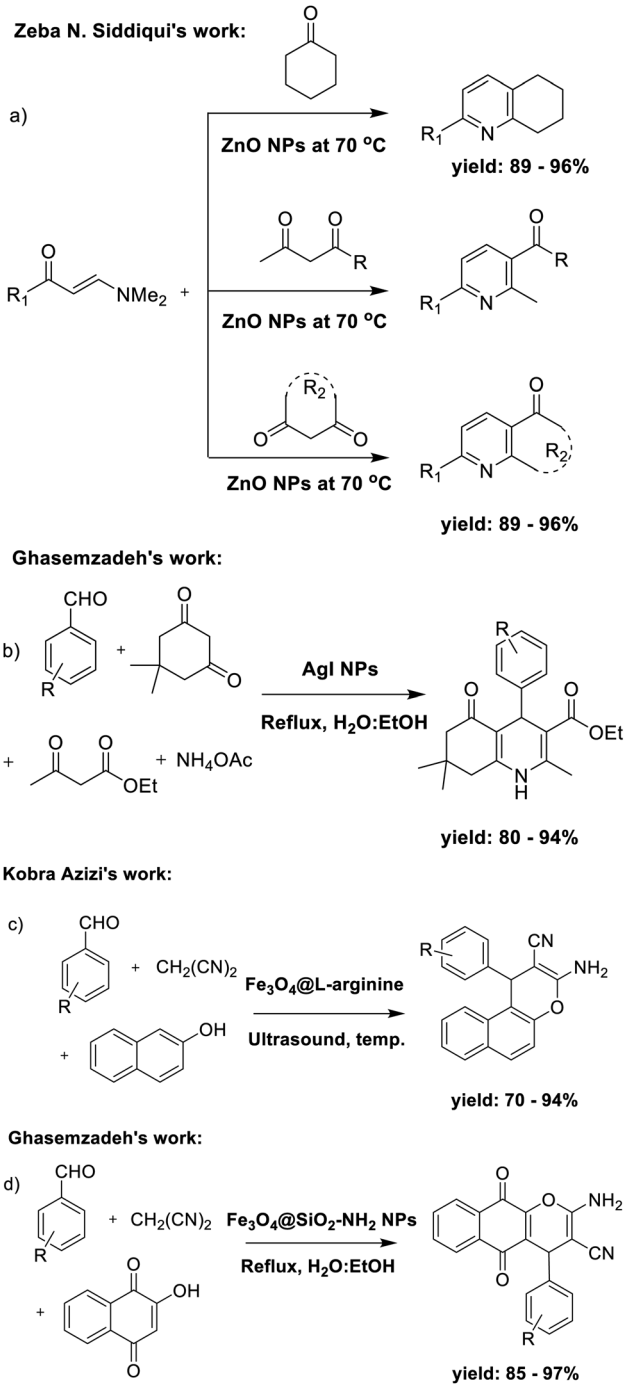

Scheme 1 Synthesis of pyridines and chromenes.

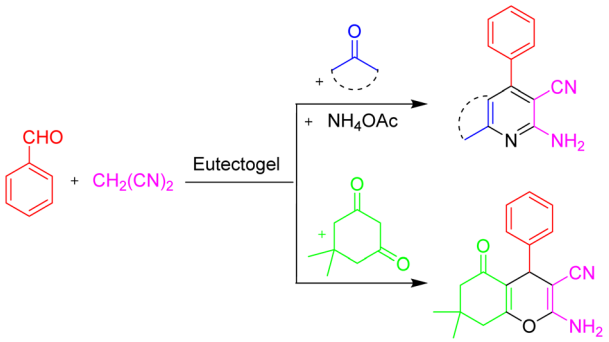

Scheme 2 The general reaction for the preparation of pyridine and chromene structure through the use of ETG.

Chromenes and their derivatives also have considerable significance due to their diverse array of biological activities,[31] including antibacterial properties,[32] sex pheromone effects,[33] anticancer potential, cancer therapeutic applications,[34] and central nervous system activity.[35] With these potential advantages, various methods have been developed in recent years to create chromene derivatives.[36] In 2014, Kobra Azizi *et al.* applied L-arginine-functionalized magnetic nanoparticles as a reusable organocatalyst with the assistance of ultrasound irradiation in the synthesis of chromenes (Scheme 1c).[37] In some following years, Ghasemzadeh *et al.*, in 2017, presented the magnetite nanoparticles-supported APTES as a powerful and recoverable nanocatalyst for the preparation of 2-amino-5,10-dihydro-5,10-dioxo-4*H*-benzo[*g*]chromenes (Scheme 1d).[38]

In this study, we present the first-time preparation of four-component ETGs for the preparation of pyridine and chromene structures (Scheme 2). A novel copolymeric deep eutectic solvent (DES) was successfully synthesized, consisting of choline chloride (HBA) as the hydrogen bond acceptor, acetamide (HBD) as the hydrogen bond donor, tetraethyl orthosilicate (TEOS), and formic acid. Then, the mixture was put under UV irradiation (254 nm) for the copolymerization process, resulting in the formation of the eutectogel. Moreover, ETGs can be applied for the preparation of pyridine and chromene structures as a reusable green catalyst through an one-pot, multi-component pathway without solvents.

Results and discussion

The present investigation involved the successful synthesis of eutectogel using choline chloride, acetamide, tetraethyl orthosilicate (TEOS), and formic acid. The molar ratio of these components was maintained at 1 : 1 : 1 : 8.7, as illustrated in Fig. 1. The copolymerization process was conducted using 254 nm UV light for 2 hours, resulting in the formation of ETG-acetamide.

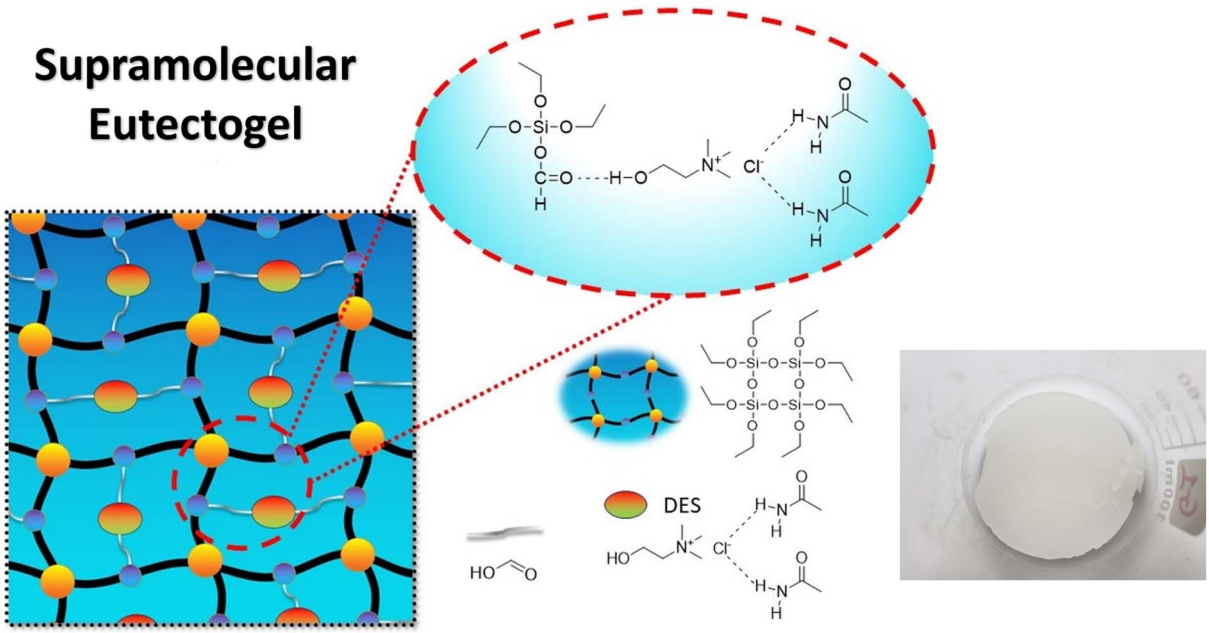

Fig. 1 The structure of ETG-acetamide.

Fig. 2 displays the Fourier Transform Infrared (FTIR) spectra of acetamide, choline chloride (ChCl), formic acid (FA), tetraethyl orthosilicate (TEOS), and ETG-acetamide. The Fourier Transform Infrared (FTIR) spectrum of pure acetamide exhibits a prominent peak at 1650 cm^{-1}, which can be attributed to the carbonyl group (C═O) in acetamide. Additionally, the bands observed at 1430, 1470, and 1540 cm^{-1} can be associated with the amide group (CON) of the CH_3CONH moiety. Choline chloride in its pure form exhibits by various functional groups. The vibrational bands observed at 3200 cm^{-1} and 1200–880 cm^{-1} correspond to the presence of a hydroxyl or amino group, specifically the stretching of N–H bonds in the former and the stretching of C–N and symmetric stretching in the latter. Additionally, the vibrational bands observed at 2980–2855 cm^{-1} and 1480–1425 cm^{-1} indicate the presence of an alkyl group, with the bending of CH_2 bonds occurring at 1485 cm^{-1}. Formic acid, within this group of bands, it is worth highlighting the prominent adsorption bands of the bidentate formate ion, specifically the COO band at 1370 cm^{-1}. The adsorption bands observed at wavenumbers 3185, 2945, 1728, and 1380 cm^{-1} can be attributed to the distinctive vibrations of OH, CH, C═O, and CH, respectively, in the H-bonded formic acid molecule. The adsorption bands observed at wavenumbers 2946, 2883, and 1665 cm^{-1} can be ascribed to the vibrations of CH and C═O in HCOOH molecules that are coordinatively bound to Lewis acid sites. The Fourier Transform Infrared (FTIR) spectra of the samples displayed distinct peaks that are indicative of tetraethyl orthosilicate (TEOS). The presence of a wide spectral band observed at a wavenumber of 3400 cm^{-1} can be attributed to the molecular water molecules forming hydrogen bonds with both other water molecules and SiOH groups. The peak observed at 1630 cm^{-1} can be attributed to the vibrational motion of water molecules. The spectral bands detected at wavenumbers 1090, 800, and 465 cm^{-1} corresponded to the vibrational modes associated with asymmetric, symmetric, and bonding characteristics of Si–O–Si bridging sequences, respectively. The vibrational patterns that are typically found in the Fourier Transform Infrared spectra of ETG-acetamide are presented and summarized in Fig. 2. It is seen that the strength of the adsorption bands in the range of 1728 to 1000 cm^{-1} for the ETG-acetamide is greater in comparison to the four-components. This difference in intensity can be attributed to the superposition of the strongly absorbing vibrations of the SiO_2 framework in this specific spectral area. The aforementioned explanation applies to the adsorption

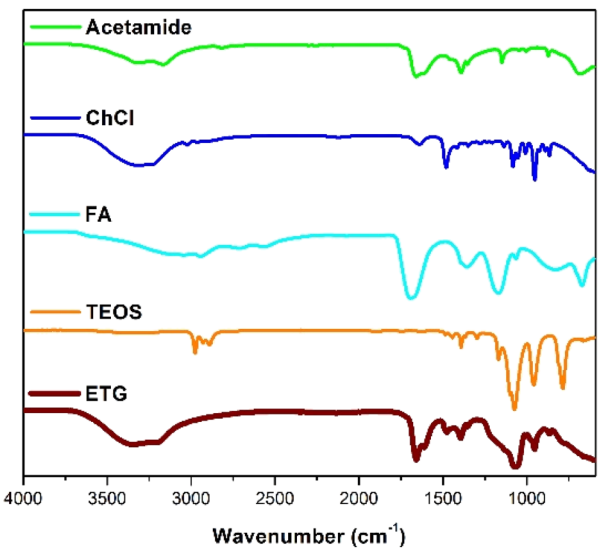

Fig. 2 FT-IR spectra of four components and ETG-acetamide.

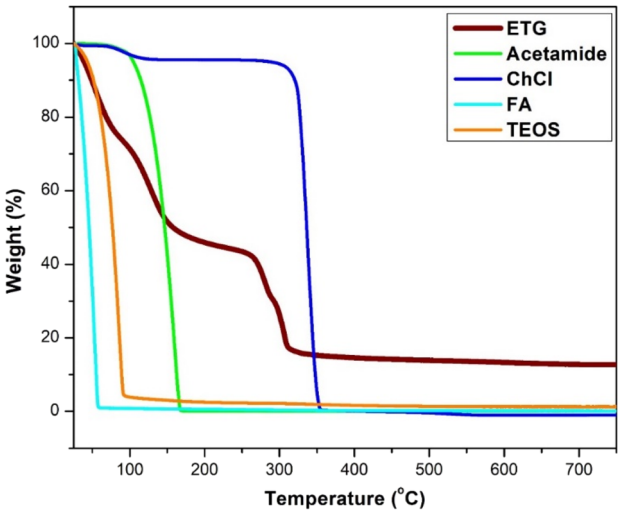

Fig. 3 TGA curve of four components and ETG-acetamide.

bands within the spectral range of 3600 to 3000 cm^{-1}. The FT-IR analysis of ETG-acetamide revealed new peaks at 866 cm^{-1}, 953 cm^{-1} and 1394 cm^{-1}, indicating the presence of C–N^+ stretching and CH_3 bending from DES,[15,39–41] confirming the successful incorporation of ETG-acetamide.

The thermal stability of choline chloride (ChCl), acetamide, tetraethyl orthosilicate (TEOS), formic acid (FA), and ETG-acetamide was studied by thermogravimetric analysis (TGA) (Fig. 3). The resulting curve exhibited an initial decrease in weight below 100 °C, which can be attributed to the elimination of adsorbed solvents, gases, and water. The second weight loss observed at temperatures over 150 °C was ascribed to the cleavage of polymer bonds within the molecule and the degradation of organic components by the catalyst. Consequently, the analysis of the TGA curve indicated that the synthesized catalyst remained stable when exposed to temperatures up to 100 °C. Moreover, ETG-acetamide exhibited efficient performance in facilitating diverse organic transformations at varying temperatures.[15] Fig. 4 illustrates the X-ray diffraction (XRD) patterns of ETG-acetamide, revealing the presence of peaks throughout the examined range of 2θ degrees, specifically between 15 and 35°, corresponds to the standard crystal plane (101) seen in semicrystalline ETG-acetamide.[42,43] The utilization of scanning electron microscopy (SEM) was employed to examine the ETG-acetamide samples, as depicted in Fig. 5. The SEM analysis revealed that the ETG-acetamide samples exhibited visual similarity in all cases, with a consistent diameter of 50 μm. The likely cause can be attributed to agglomeration. The confirmation of the presence of silicon (Si) atoms within these nuclei was achieved through the utilization of energy dispersive X-ray (EDX) research (Fig. 6). In addition, Brunauer–Emmett–Teller (BET) analysis method was also applied to ETG-acetamide material, the results are presented in Fig. S1 (ESI†), the specific surface area (0.5751 $m^2\ g^{-1}$) and pore volume (0.000008 $cm^3\ g^{-1}$).

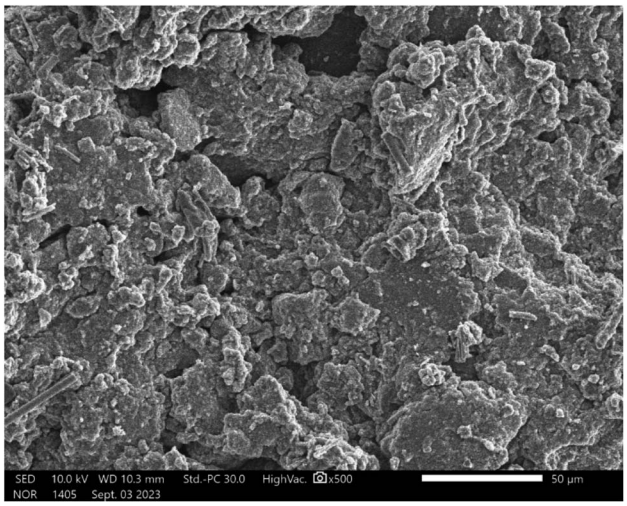

Fig. 5 SEM for ETG-acetamide.

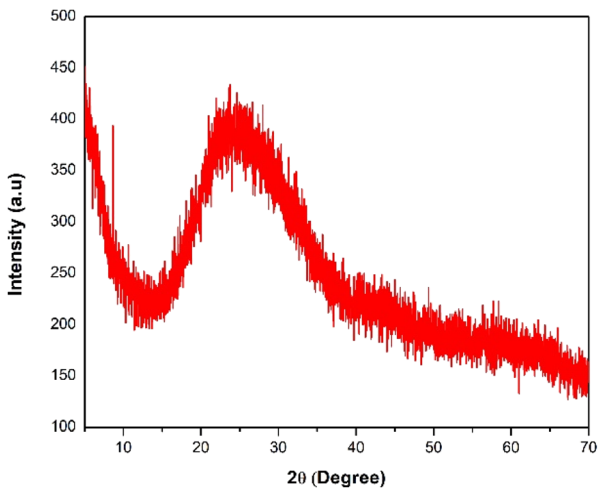

Fig. 4 XRD pattern for ETG-acetamide.

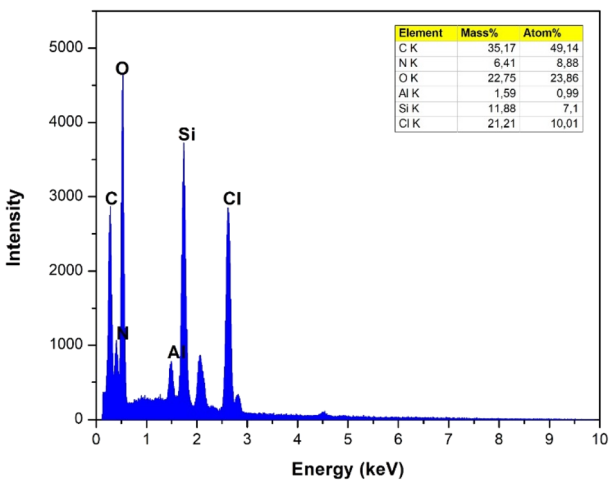

Fig. 6 Energy-dispersive X-ray spectroscopy for ETG-acetamide.

Table 1 Optimizing the conditions of the model reaction's synthesis[a]

Entry	Temperature (°C)	Time (h)	Yield[b] (%)
1	100	2	50
2	70	2	45
3	80	2	62
4	120	2	45
5	140	2	40
6	160	2	37
7	160	2	37
8	80	0.5	55
9	80	1	56
10	80	2	59
11	80	2.5	61
12	80	2.75	64
13	**80**	**3**	**71**
14	80	3.25	65
15	80	3.5	53

[a] Reaction conditions: malononitrile (1 mmol), benzaldehyde (1 mmol), ammonium acetate (1.5 mmol), cyclohexanone (1 mmol), and ETG-acetamide (50 mg). [b] Isolated yield by crystallization in ethanol (10–15 mL).

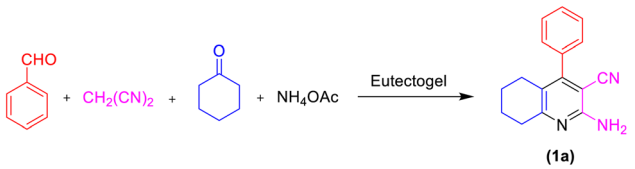

Scheme 3 Synthesis of (**1a**).

The factors investigated in this research were the ETG-acetamide loading, heating temperature, and reaction duration. Table 1 displays a detailed overview of the most noteworthy results derived from the investigation.

In the present study, we selected the model reaction involving malononitrile (1 mmol), benzaldehyde (1 mmol), ammonium acetate (1.5 mmol), and cyclohexanone (1 mmol) in the presence of ETG-acetamide through four-component reaction with the objective of synthesizing 2-amino-4-phenyl-5,6,7,8-tetrahydroquinoline-3-carbonitrile (**1a**) (Scheme 3). This research also aimed to optimize the reaction parameters and determine the appropriate conditions (Table 1).

The preparation of the product was examined by modifying different reaction conditions. The reaction temperature was varied, ranging from 70 to 160 °C. Furthermore, the reaction time was adjusted to durations of 0.5 to 3.5 hours and these conditions include the quantity of ETG-acetamide used. The progress of the product formation was monitored through the use of Thin-Layer Chromatography (TLC). The experimental findings were documented in Table 1, which demonstrated that the optimal product yield could be achieved by conducting the reaction at a temperature of 80 °C, utilizing a catalyst amount of 50 mg, and allowing the reaction to proceed for a duration of 3 hours (Table 1, entry 13). The experiments focus on determining the quantity of ETG-acetamide utilised and the ideal weight of the catalyst, both of which amount to 50 mg (Fig. 7).

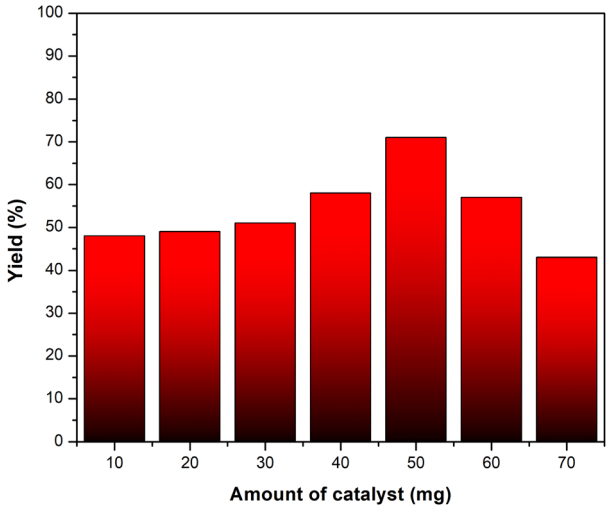

Fig. 7 The investigation of influence of ETG-acetamide weight.

Following that, other catalysts including ETG-$ZrOCl_2 \cdot 8H_2O$, ETG-benzamide, and other DESs were investigated (Table 2). The catalytic effect of the Lewis-base catalyst effectively facilitated the transformation, exhibiting notable efficacy. Among them, ETG-acetamide also exhibited the most favourable catalytic performance, resulting in a product yield of 71% for **1a** (Table 2, entry 1). In contrast, just a small quantity of the intended product was detected during the execution of the reaction employing a Lewis-acid ETG-$ZrOCl_2 \cdot 8H_2O$ catalyst (Table 2, entry 3) or ChCl : imidazole (3 : 7), ChCl : *p*-phenylenediamine (1 : 2), without catalyst (Table 2, entries 10–11 and

Table 2 Investigating the influence of catalyst for the synthesis of (**1a**).[a]

Entry	Catalysts/solvents	Yield[b] (%)
1	**ETG-acetamide**[c]	**71**
2	ETG-benzamide[c]	39
3	ETG-$ZrOCl_2 \cdot 8H_2O$[c]	Trace
4	ChCl : urea (1 : 1)[c]	58
5	ChCl : urea (1 : 2)[c]	66
6	ChCl : acetamide (1 : 2)[c]	67
7	ChCl : benzamide (1 : 2)[c]	45
8	ChCl : indole (1 : 2)[c]	61
9	ChCl : 2-aminobenzimidazole (1 : 2)[c]	37
10	ChCl : imidazole (3 : 7)[c]	Trace
11	ChCl : *p*-phenylenediamine (1 : 2)[c]	Trace
12	Tetraethyl orthosilicate[c]	Trace
13	Choline chloride[c]	10
14	Formic acid[c]	Trace
15	Ethyl acetate (EtOAc)[d]	Trace
16	Acetone[d]	Trace
17	EtOH[d]	Trace
18	None	Trace

[a] Reaction conditions: malononitrile (1 mmol), benzaldehyde (1 mmol), ammonium acetate (1.5 mmol), cyclohexanone (1 mmol). [b] Isolated yield by crystallization in ethanol (10–15 mL). [c] Catalysts (50 mg), solvent-free, at 80 °C. [d] Solvent (5 mL), ETG-acetamide (50 mg), at room temperature.

Table 3 The synthesis of pyridine derivatives (**1a–15a**) catalyzed by ETG-acetamide[a]

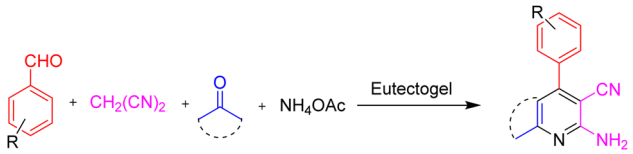

Entry	R	Ketone	Product	Time (h)	Yield[a] (%)	Mp. (°C)	Ref.
1a	H	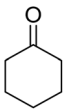	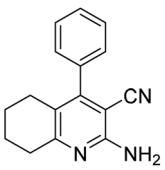	3	71[b]	242–244	237–239 (ref. 44)
2a	4-OMe	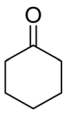	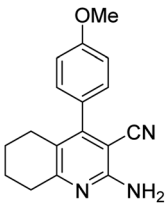	3	47[b]	239–240	234–236 (ref. 45)
3a	4-Cl	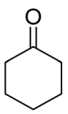	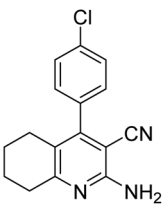	3	33[b]	266–268	260–261 (ref. 45)
4a	4-F	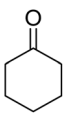	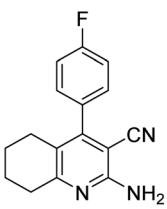	3.5	58[b]	259–260	—
5a	2-Cl	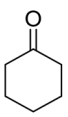	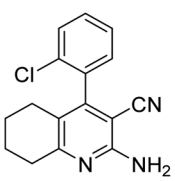	3	46[b]	259–261	254–257 (ref. 46)
6a	2-F	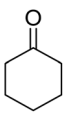	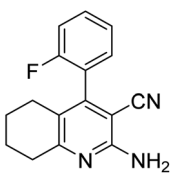	3	44[b]	254–256	—
7a	4-Br	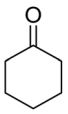	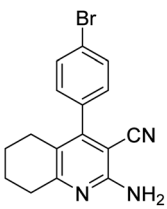	3	53[b]	299–301	255–257 (ref. 45)

Table 3 (*Contd.*)

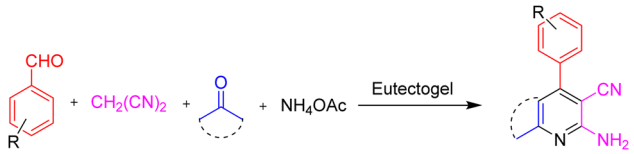

Entry	R	Ketone	Product	Time (h)	Yield[a] (%)	Mp. (°C)	Ref.
8a	4-Me	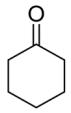	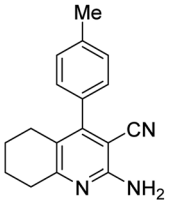	3	44[b]	258–260	256–258 (ref. 46)
9a	Furfural	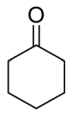	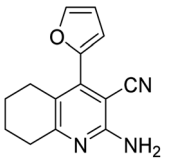	3	48[b]	216–218	—
10a	H	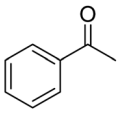	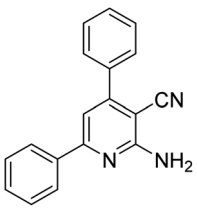	2.5	15[c]	186–187	185–187 (ref. 47)
11a	4-OMe	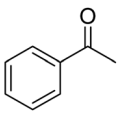	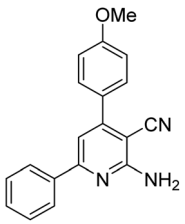	2.5	12[c]	188–190	192–195 (ref. 48)
12a	4-Cl	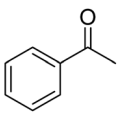	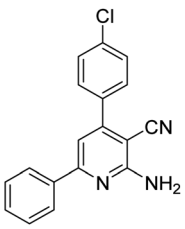	3	46[c]	185–186	203–205 (ref. 49)
13a	4-F	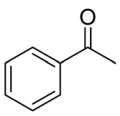	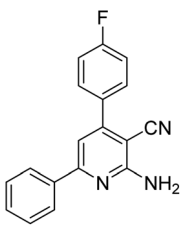	3	19[c]	164–166	164–166 (ref. 50)

Table 3 (*Contd.*)

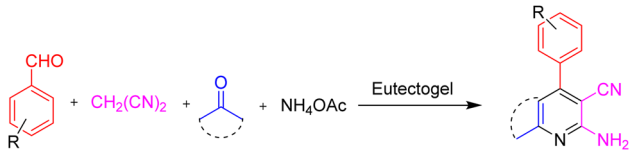

Entry	R	Ketone	Product	Time (h)	Yield[a] (%)	Mp. (°C)	Ref.
14a	4-Br	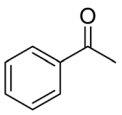	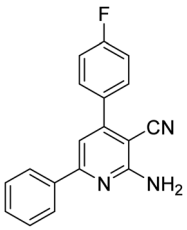	3	36[c]	183–185	186–188 (ref. 50) 215–217 (ref. 49) 231–233 (ref. 51)
15a	4-Me	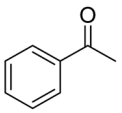	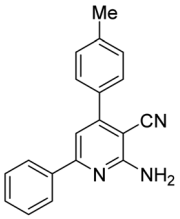	3	31[c]	210–212	

[a] Reaction conditions: arylaldehyde (1 mmol), malononitrile (1 mmol), cyclohexanone/dimedone (1 mmol), ammonium acetate (1.5 mmol), ETG-acetamide (50 mg) at 80 °C. [b] Isolated yield by crystallization in ethanol (10–15 mL). [c] Isolated yield *via* column chromatography (*n*-hexane : EtOAc = 5 : 5).

18). On the other hand, each substance used for the synthesis of eutectogel is also reported to determine the performance of ETG-acetamide (Table 2, entries 12–14).

Therefore, the indicated optimal conditions were used to synthesize further pyridine derivatives (Table 3) and chromene derivatives (Table 4) following the overall reaction described in Scheme 2.

As can be seen in Table 3, the substituted aromatic aldehydes, which can have electron-donating groups (*e.g.*, Me and OMe) or electron-withdrawing groups (*e.g.*, Cl, F, Br, and NO_2), underwent a reaction at the *para* position. This reaction resulted in the formation of the corresponding 2-amino-4-phenyl-5,6,7,8-tetrahydroquinoline-3-carbonitriles with high yields (entries **1a–9a**, Table 3). The substitution of cyclohexanone with acetophenone did not result in a substantial alteration in the yield of product production (entries **10a–15a**, Table 3).

The aldehyde, malononitrile, and dimedone underwent a reaction under identical experimental conditions, and the outcomes are presented in Table 4. The presence of two carbonyl groups in dimedone results in the synthesis of the compound 2-amino-7,7-dimethyl-5-oxo-4-phenyl-5,6,7,8-tetrahydro-4*H*-chromene-3-carbonitrile frames. The substitution of different aromatic aldehydes, which contain groups that either donate or withdraw electrons (*e.g.*, Me, OMe, Cl, F, and Br), at the *para* position resulted in the formation of 2-amino-7,7-dimethyl-5-oxo-4-phenyl-5,6,7,8-tetrahydro-4*H*-chromene-3-carbonitriles with high yields (entries **16b–22b**, Table 4).

However, depending on certain derivative compounds, the reaction time was prolonged to 4 hours with the intention of improving the total yield of the reaction. The general synthetic reaction could also be scaled up to 10 mmol with a slight decrease compared to 1 mmol. As a result, the possibility for industrial-scale production exists for the pyridine preparation process (Fig. 8).

A plausible mechanism elucidating the synthesis of pyridine (**Va**) and chromene (**IIIb**) employing ETG-acetamide is depicted in Scheme 4, comprising three stages. Initially, it is postulated that the reaction proceeds through a Knoevenagel condensation mechanism, wherein malononitrile reacts with the carbonyl group of aldehyde under ETG-acetamide catalyst. This results in the formation of an intermediate compound known as 2-benzylidenemalononitrile (**I**), accompanied by the elimination of a water molecule.[54] In the subsequent step, the dimedone undergoes Michael addition, resulting in the conversion to its enol form. Following tautomerization, the enol form then acts as an acceptor, attacking the intermediate **I**. This reaction yields the formation of intermediate **IIa** and **IIb**.[55] The last step of the reaction synthesizing pyridine entails the generation of enaminone **IIIa** through the reaction between the carbonyl group in the ketone and an excess of ammonium acetate, but this phenomenon does not happen with **IIb**.[52,56] Subsequently, an

Table 4 The synthesis of different derivatives (**16b–23b**) of chromene structure catalyzed by ETG-acetamide[a]

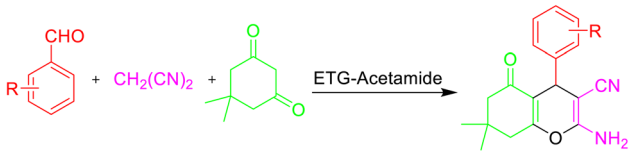

(**16b-23b**)

Entry	R	Ketone	Product	Time (h)	Yield[a] (%)	Mp. (°C)	Ref.
16b	H	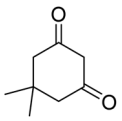	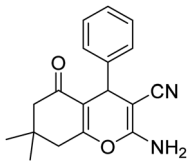	3	50[b]	233–234	228–230 (ref. 52)
17b	4-OMe	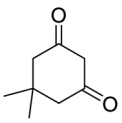	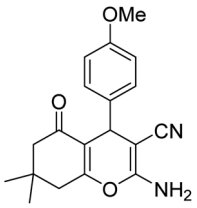	3	14[c]	200–202	197–199 (ref. 53)
18b	4-F	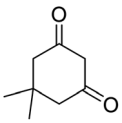	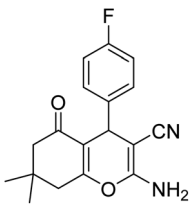	4	75[b]	184–185	191–193 (ref. 53)
19b	2-Cl	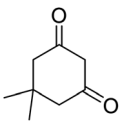	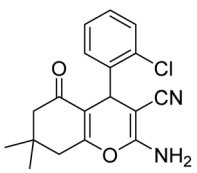	3	7[c]	213–215	211–213 (ref. 52)
20b	2-F	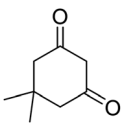	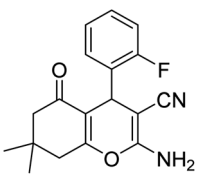	3	42[b]	237–239	—
21b	4-Br	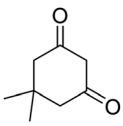	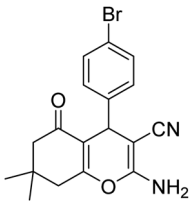	3	8[c]	232–234	216–218 (ref. 52)
22b	4-Me	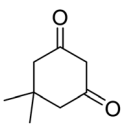	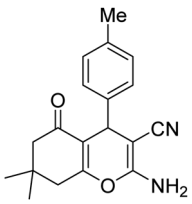	3	6[c]	200–202	218–220 (ref. 52)

Table 4 (*Contd.*)

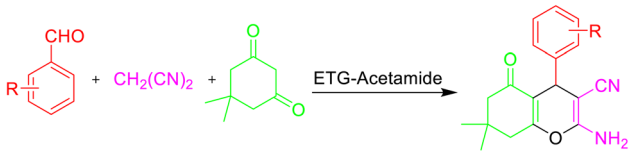

(**16b-23b**)

Entry	R	Ketone	Product	Time (h)	Yield[a] (%)	Mp. (°C)	Ref.
23b	Furfural	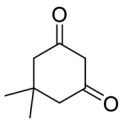	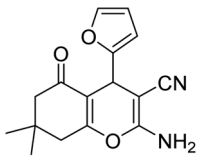	3	28[b]	218–220	—

[a] Reaction conditions: arylaldehyde (1 mmol), malononitrile (1 mmol), cyclohexanone/dimedone (1 mmol), ETG-acetamide (50 mg) at 80 °C. [b] Isolated yield by crystallization in ethanol (10–15 mL). [c] Isolated yield *via* column chromatography (*n*-hexane : EtOAc = 5 : 5).

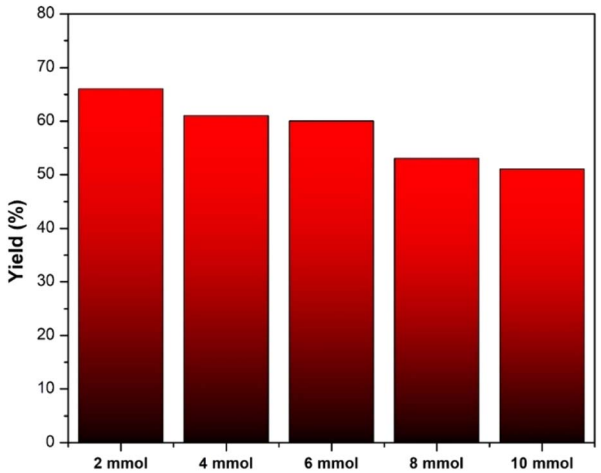

Fig. 8 Large-scale synthesis of (**1a**).

intramolecular cyclization mechanism ensues, leading to the formation of the intended product, pyridine **IVa** and chromene **IIIb** structure.[57,58] The formation of **Va** occurs *via* the anomeric-based oxidation (ABO) mechanism, involving the elimination of a single water molecule.[59]

The control reactions were also conducted to prove the reasonableness of the mechanism proposed. The result showed that the first appropriate step to synthesize the desired product is the formation of 2-benzylidenemalononitrile (**I**) (Table S1,† entry 1), which was isolated from the reaction and determined *via* ^{1}H-NMR spectra to confirm the structure (Fig. S2 and 24.1†).

The feasibility of recycling the ETG-acetamide compound was investigated by subjecting it to the reaction of (**1a**) under the conditions that we have optimized. Following the conclusion of the reaction, a quantity of EtOAc (10–15 mL) was introduced into the reaction mixture and subsequently retrieved through the process of filtration. The solid obtained was subjected to a series of washes using water (5 × 3 mL), and acetone (5 × 3 mL), followed by drying under vacuum. According to the data presented in Fig. 9, it was seen that the catalyst exhibited the potential for reusability, with the ability to be utilized for up to three consecutive cycles while achieving yields exceeding 45%. The structure of the catalyst was confirmed by FTIR spectrum, the results are shown in the Fig. 10.

Table 5 demonstrates that while all of the aforementioned catalysts are suitable for the specified synthetic conditions, the majority of them have certain disadvantages. These drawbacks include elevated temperatures, extended reaction durations, excessive catalyst amounts, utilization of toxic catalysts or toxic organic solvents, and laborious work-up procedures.

Experimental

Chemical

Benzaldehyde (99%), 4-methoxybenzaldehyde (98%), 4-chlorobenzaldehyde (98%), 4-fluorobenzaldehyde (98%), 2-fluorobenzaldehyde (97%), 4-bromobenzaldehyde (99%), 4-methylbenzaldehyde (97%), 2-furaldehyde (99%), ammonium acetate (97%), 2-chlorobenzaldehyde (99%) were purchased from Sigma-Aldrich. 1,3-Cyclohexadione (97%), acetophenone (98%), malononitrile (99%), and dimedone (99%) were acquired from Acros.

Ethyl acetate (for analysis EMSURE ACS, ISO, Reag. Ph Eur) and acetone (for analysis EMPARTA ACS) were acquired from Merck. Thin-layer chromatography (TLC) was conducted using aluminum plates (F-254) covered with silica gel. The experiment included the use of silica gel (230–400 mesh, Merck) for column chromatography.

Techniques for analysis

The ^{1}H-NMR and ^{13}C-NMR spectra were acquired utilizing a Bruker Avance 500 MHz instrument using DMSO-d_6 as the

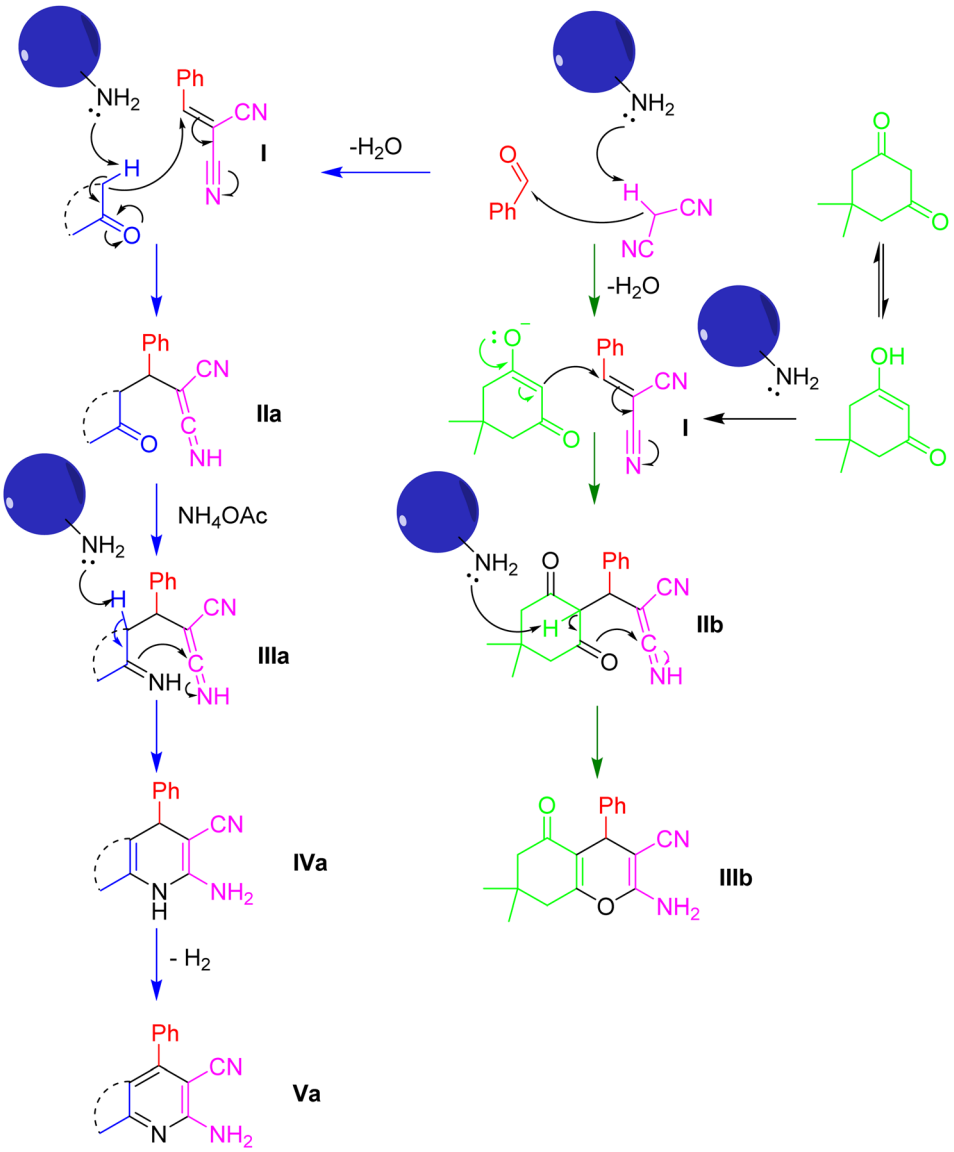

Scheme 4 The suggested mechanism for the synthesis of pyridine (**Va**) and chromene (**IIIb**) structures using ETG-acetamide.

solvent peaks serving as the system's internal standard. The melting points were determined utilizing a Buchi B-545 melting point apparatus. Fourier-transform infrared (FT-IR) spectra were acquired using a Bruker E400 FT-IR spectrometer. Thermogravimetric analysis (TGA) was carried out using a Q-500 apparatus. The experimental procedure included exposing the sample to a temperature gradient at a rate of 5 °C per minute while maintaining a controlled airflow. The refining process included the acquisition of Powder X-ray diffraction (P-XRD) data using a Bruker D8 Advance instrument. The data was obtained by employing Ni-filtered Cu K ($\lambda = 1.54059$) radiation. The shape and structure of the material were examined with a Hitachi S-4800 scanning electron microscopy (SEM) in combination with an XZS-107T digital microscope and an NHV-CAM camera, aided by the eScope software. The N_2 isotherm was measured and analyzed using the Quantachrome NOVA 3200e system, which operated at a temperature of 77 K. The EMAX energy EX-400 EDX device was used to perform an examination using energy-dispersive X-ray spectroscopy (EDX). The high-resolution mass spectra were acquired using a Bruker micrOTOF-QII mass spectrometer, which was operated in positive electrospray ionization mode and had an ionization energy of 80 electron volts (eV).

Preparation of ETG

Choline chloride, acetamide, tetraethyl orthosilicate (TEOS), and formic acid were sequentially introduced into a round-bottom flask equipped with a magnetic stirrer, maintaining a molar ratio of 1 : 1 : 1 : 8.7. Following this, the mixture of reactants underwent agitation at a temperature of 60 °C in an unsealed environment until a uniform mixture was achieved. The mix of ingredients was let to cool for roughly five minutes at atmospheric temperature. Upon completion of the reaction, the

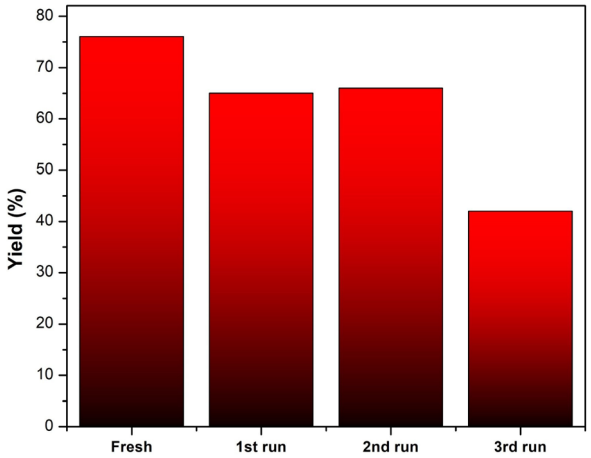

Fig. 9 Catalytic activity of ETG-acetamide in three cycles for the reaction of (**1a**) under our optimized conditions.

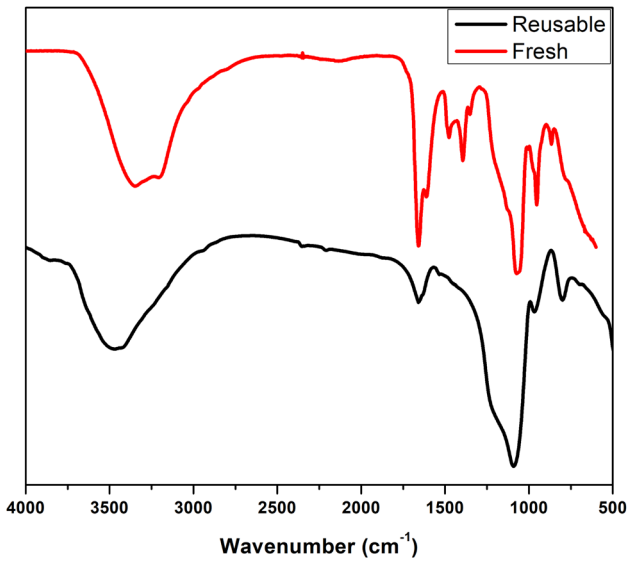

Fig. 10 FT-IR spectrum of ETG-acetamide fresh (red) and reusable (after 3 times) (black).

copolymerization process was carried out using UV light irradiation at a wavelength of 254 nm for a period of 2 hours. This led to the synthesis of the eutectogel. The gel underwent solidification, resulting in the formation of a solid mass. Subsequently, the mixture was left to evaporate naturally for a duration of 14 days. Following this, ETG-acetamide was obtained. The confirmation of characteristics and structural integrity was conducted by the use of several analytical techniques, including FT-IR, XRD, TGA, EDS, and SEM.

The synthetic process of pyridine and chromene compounds following a general approach

A mixture containing of arylaldehyde (1 mmol), malononitrile (1 mmol), and ETG-acetamide (50 mg) was exposed to agitation at 80 °C for a period of 10 to 15 minutes. Subsequently, a mixture containing ketone/dimedone (1 mmol) and/or ammonium acetate (1.5 mmol) was put into the container of the mixture. The reaction mixture obtained was subjected to continual mixing for 3 hours at a specified temperature of 80 °C. Throughout the stirring process, the advancement of the reaction was assessed by TLC (*n*-hexane–EtOAc = 1 : 1). The mixture was put through dilution using 15–20 mL of EtOAc and then filtered using filter paper. The organic liquid was subjected to cooling in order to induce crystallization at ambient temperature, or alternatively, silica gel served as the stationary phase throughout the purification process that used column chromatography. The products were determined *via* the use of melting point, ^{1}H-NMR, ^{13}C-NMR spectra.

2-Amino-4-phenyl-5,6,7,8-tetrahydroquinoline-3-carbonitrile[64] (1a). Yield 71%, the pale yellow powder. R_f = 0.59 (*n*-hexane–EtOAc = 5 : 5); Mp. = 242–244 °C; ^{1}H-NMR (500 MHz, DMSO-d_6): δ = 1.55–1.60 (m, 2H), 1.70–1.75 (m, 2H), 2.19 (t, J = 6.5 Hz, 2H), 2.70 (t, J = 6.5 Hz, 2H), 5.64 (s, 2H), 7.26–7.28 (m, 2H), 7.44–7.46, (m, 1H), 7.48–7.51 (m, 2H) ppm. ^{13}C-NMR (125 MHz, DMSO-d_6): δ = 22.1, 22.4, 25.8, 32.8, 88.0, 116.7, 118.3, 128.0, 128.5, 128.6, 136.4, 153.9, 157.9, 160.9 ppm.

2-Amino-4-(4-methoxyphenyl)-5,6,7,8-tetrahydroquinoline-3-carbonitrile[46] (2a). Yield 47%, the pale yellow powder. R_f = 0.51 (*n*-hexane–EtOAc = 5 : 5); Mp. = 239–240 °C; ^{1}H-NMR (500 MHz, DMSO-d_6): δ = 1.55–1.59 (m, 2H), 1.70–1.75 (m, 2H), 2.23 (t, J = 6.5 Hz, 2H), 2.69 (t, J = 6.5 Hz, 2H), 3.81 (s, 3H), 6.51 (s, 2H), 7.04 (d, J = 8.5 Hz, 2H), 7.22 (d, J = 8.5 Hz, 2H) ppm. ^{13}C-NMR (125 MHz, DMSO-d_6): δ = 22.1, 22.5, 25.9, 32.8, 55.1, 88.3, 113.9, 116.9, 118.6, 128.5, 129.6, 153.7, 157.9, 159.3, 160.8 ppm.

2-Amino-4-(4-chlorophenyl)-5,6,7,8-tetrahydroquinoline-3-carbonitrile[46] (3a). Yield 33%, the yellow powder. R_f = 0.53 (*n*-hexane–EtOAc = 5 : 5); Mp. = 266–268 °C; ^{1}H-NMR (500 MHz, DMSO-d_6): δ = 1.56–1.61 (m, 2H), 1.71–1.75 (m, 2H), 2.19 (t, J =

Table 5 Comparison of some other procedures with the present method for the synthesis of **1a**

Entry	Catalysts	Temperature (°C)	Time (h)	Yield (%)	Ref.
1	Trifluoroethanol (TFE) (2 mL)	Reflux	6	80	60
2	1-Butyl-3-methylimidazolium hydroxide (2 mL)	80	4	82	61
3	Cu/C nanocatalyst (2 mol%), CH_3CN (2 mL)	80	8	84	62
4	Graphene oxide (10 mol%)/water (3 mL)	80	5	86	63
5	ETG-acetamide (50 mg)	80	3	71	This work

6.5 Hz, 2H), 2.70 (t, J = 6.5 Hz, 2H), 6.60 (s, 2H), 7.34 (d, J = 8.5 Hz, 2H), 7.57 (d, J = 8.5 Hz, 2H) ppm. ^{13}C-NMR (125 MHz, DMSO-d_6): δ = 22.0, 22.4, 25.8, 32.8, 87.8, 116.5, 118.2, 128.7, 130.1, 133.4, 135.2, 152.7, 157.9, 161.1 ppm.

2-Amino-4-(4-fluorophenyl)-5,6,7,8-tetrahydroquinoline-3-carbonitrile (4a). Yield 58%, the pale yellow powder. R_f = 0.52 (n-hexane–EtOAc = 5 : 5); Mp. = 259–260 °C; ^{1}H-NMR (500 MHz, DMSO-d_6): δ = 1.56–1.61 (m, 2H), 1.71–1.75 (m, 2H), 2.19 (t, J = 6.5 Hz, 2H), 2.70 (t, J = 6.5 Hz, 2H), 6.58 (s, 2H), 7.33–7.37 (m, 4H) ppm. ^{13}C-NMR (125 MHz, DMSO-d_6): δ = 22.1, 22.4, 25.8, 32.8, 88.1, 115.7 (d, J = 21.3 Hz), 116.6, 118.4, 130.5 (d, J = 8.8 Hz), 132.7 (d, J = 2.5 Hz), 153.0, 157.9, 161.0, 162.1 (d, J = 243.8 Hz) ppm.

2-Amino-4-(2-chlorophenyl)-5,6,7,8-tetrahydroquinoline-3-carbonitrile[46] (5a). Yield 46%, the pale yellow powder. R_f = 0.59 (n-hexane–EtOAc = 5 : 5); Mp. = 259–251 °C; ^{1}H-NMR (500 MHz, DMSO-d_6): δ = 1.57–1.63 (m, 2H), 1.70–1.75 (m, 2H), 2.03–2.14 (m, 2H), 2.66–2.77 (m, 2H), 6.66 (s, 2H), 7.31–7.32 (m, 1H), 7.48–7.50 (m, 2H), 7.62–7.63 (m, 1H) ppm. ^{13}C-NMR (125 MHz, DMSO-d_6): δ = 22.1, 22.2, 25.2, 32.7, 87.9, 116.1, 118.5, 127.7, 129.6, 129.9, 130.5, 131.0, 135.2, 151.3, 157.8, 161.3 ppm.

2-Amino-4-(2-fluorophenyl)-5,6,7,8-tetrahydroquinoline-3-carbonitrile (6a). Yield 44%, the yellow powder. R_f = 0.58 (n-hexane–EtOAc = 5 : 5); Mp. = 254–256 °C; ^{1}H-NMR (500 MHz, DMSO-d_6): δ = 1.58–1.63 (m, 2H), 1.71–1.76 (m, 2H), 2.09–2.24 (m, 2H), 2.66–2.77 (m, 2H), 6.66 (s, 2H), 7.33–7.39 (m, 3H), 7.52–7.56 (m, 1H) ppm. ^{13}C-NMR (125 MHz, DMSO-d_6): δ = 22.0, 22.2, 25.3, 32.7, 88.3, 115.9 (d, J = 21.3 Hz), 116.2, 118.9, 123.6 (d, J = 17.5 Hz), 124.9 (d, J = 2.5 Hz), 129.6 (d, J = 2.5 Hz), 131.3 (d, J = 8.8 Hz), 148.0, 157.8, 158.2 (d, J = 242.5 Hz), 161.3 ppm.

2-Amino-4-(4-bromophenyl)-5,6,7,8-tetrahydroquinoline-3-carbonitrile[45] (7a). Yield 53%, the pale yellow powder. R_f = 0.53 (n-hexane–EtOAc = 5 : 5); Mp. = 299–301 °C; ^{1}H-NMR (500 MHz, DMSO-d_6): δ = 1.58–1.62 (m, 2H), 1.71–1.75 (m, 2H), 2.19 (t, J = 6.5 Hz, 2H), 2.70 (t, J = 6.5 Hz, 2H), 6.61 (s, 2H), 7.27 (d, J = 8.5 Hz, 2H), 7.70 (d, J = 8.5 Hz, 2H) ppm. ^{13}C-NMR (125 MHz, DMSO-d_6): δ = 22.0, 22.4, 25.8, 32.8, 87.7, 116.5, 118.1, 122.1, 130.4, 131.6, 135.6, 152.7, 157.9, 161.1 ppm.

2-Amino-4-(*p*-tolyl)-5,6,7,8-tetrahydroquinoline-3-carbonitrile[46] (8a). Yield 44%, the pale yellow powder. R_f = 0.57 (n-hexane–EtOAc = 5 : 5); Mp. = 258–260 °C; ^{1}H-NMR (500 MHz, DMSO-d_6): δ = 1.54–1.59 (m, 2H), 1.70–1.75 (m, 2H), 2.20 (t, J = 6.5 Hz, 2H), 2.37 (s, 3H), 2.69 (t, J = 6.5 Hz, 2H), 6.52 (s, 2H), 7.16 (d, J = 8.0 Hz, 2H), 7.30 (d, J = 8.0 Hz, 2H) ppm. ^{13}C-NMR (125 MHz, DMSO-d_6): δ = 20.8, 22.1, 22.5, 25.9, 32.8, 88.1, 116.7, 118.4, 128.0, 129.1, 133.4, 137.9, 154.0, 157.9, 160.8 ppm.

2-Amino-4-(furan-2-yl)-5,6,7,8-tetrahydroquinoline-3-carbonitrile (9a). Yield 48%, the yellow powder. R_f = 0.58 (n-hexane–EtOAc = 5 : 5); Mp. = 216–218 °C; ^{1}H-NMR (500 MHz, DMSO-d_6): δ = 0.78–0.82 (m, 2H), 0.88–0.92 (m, 2H), 1.68 (t, J = 6.0 Hz, 2H), 1.86 (t, J = 6.5 Hz, 2H), 5.74 (s, 2H), 5.86 (dd, J = 1.5 Hz, 3.5 Hz, 1H), 6.06 (d, J = 3.5 Hz, 1H), 7.08 (d, J = 1.5 Hz, 1H) ppm. ^{13}C-NMR (125 MHz, DMSO-d_6): δ = 21.9, 22.5, 26.1, 33.0, 85.7, 111.7, 113.7, 116.9, 118.3, 141.1, 144.5, 147.4, 158.5, 161.7 ppm.

2-Amino-4,6-diphenylnicotinonitrile[65] (10a). Yield 15%, the white powder. R_f = 0.84 (n-hexane–EtOAc = 5 : 5); Mp. = 186–187 °C; ^{1}H-NMR (500 MHz, DMSO-d_6): δ = 7.01 (s, 2H), 7.28 (s, 1H), 7.48–7.51 (m, 3H), 7.54–7.58 (m, 3H), 7.68 (dd, J = 2.0 Hz, 8.0 Hz, 2H), 8.12–8.14 (m, 2H) ppm. ^{13}C-NMR (125 MHz, DMSO-d_6): δ = 86.7, 109.3, 117.0, 127.3, 128.4, 128.7, 129.6, 130.1, 137.0, 137.6, 154.9, 158.6, 160.9 ppm.

2-Amino-4-(4-methoxyphenyl)-6-phenylnicotinonitrile[65] (11a). Yield 12%, the white powder. R_f = 0.78 (n-hexane–EtOAc = 5 : 5); Mp. = 188–190 °C; ^{1}H-NMR (500 MHz, DMSO-d_6): δ = 3.84 (s, 3H), 6.95 (s, 2H), 7.11 (d, J = 8.5 Hz, 2H), 7.25 (s, 1H), 7.47–7.49 (m, 3H), 7.66 (d, J = 8.5 Hz, 2H), 8.12 (dd, J = 2.5 Hz, 7.5 Hz, 2H) ppm. ^{13}C-NMR (125 MHz, DMSO-d_6): δ = 55.3, 86.4, 109.0, 114.2, 117.3, 127.2, 128.6, 129.1, 129.8, 130.0, 137.7, 154.5, 158.5, 160.4, 161.0 ppm.

2-Amino-4-(4-chlorophenyl)-6-phenylnicotinonitrile[65] (12a). Yield 46%, the white powder. R_f = 0.84 (n-hexane–EtOAc = 5 : 5); Mp. = 185–186 °C; ^{1}H-NMR (500 MHz, DMSO-d_6): δ = 7.05 (s, 2H), 7.29 (s, 1H), 7.48–7.51 (m, 3H), 7.63 (d, J = 8.5 Hz, 2H), 7.72 (d, J = 8.5 Hz, 2H), 8.12–8.14 (m, 2H) ppm. ^{13}C-NMR (125 MHz, DMSO-d_6): δ = 86.5, 109.1, 116.8, 127.3, 128.6, 128.7, 130.1, 130.3, 134.5, 135.8, 137.5, 153.6, 158.7, 160.8 ppm.

2-Amino-4-(4-fluorophenyl)-6-phenylnicotinonitrile (13a). Yield 19%, the white powder. R_f = 0.84 (n-hexane–EtOAc = 5 : 5); Mp. = 164–166 °C; ^{1}H-NMR (500 MHz, DMSO-d_6): δ = 7.0 (s, 2H), 7.28 (s, 1H), 7.38–7.43 (m, 2H), 7.48–7.51 (m, 3H), 7.73–7.77 (m, 2H), 8.12–8.14 (m, 2H) ppm. ^{13}C-NMR (125 MHz, DMSO-d_6): δ = 86.6, 109.3, 115.7 (d, J = 22.5 Hz), 117.0, 127.3, 128.6, 130.1, 130.8 (d, J = 8.8 Hz), 133.4 (d, J = 2.5 Hz), 137.5, 153.8, 158.7, 160.8, 162.9 (d, J = 245.0 Hz) ppm.

2-Amino-6-phenyl-4-(4-bromophenyl)nicotinonitrile[45] (14a). Yield 36%, the white powder. R_f = 0.84 (n-hexane–EtOAc = 5 : 5); Mp. = 183–185 °C; ^{1}H-NMR (500 MHz, DMSO-d_6): δ = 7.05 (s, 2H), 7.28 (s, 1H), 7.48–7.51 (m, 3H), 7.64 (d, J = 8.5 Hz, 2H), 7.77 (d, J = 8.5 Hz, 2H), 8.12–8.14 (m, 2H) ppm. ^{13}C-NMR (125 MHz, DMSO-d_6): δ = 86.4, 109.1, 116.8, 123.2, 127.3, 128.6, 130.2, 130.5, 131.7, 136.1, 137.5, 153.7, 158.8, 160.8 ppm.

2-Amino-6-phenyl-4-(*p*-tolyl)nicotinonitrile[65] (15a). Yield 31%, the white powder. R_f = 0.84 (n-hexane–EtOAc = 5 : 5); Mp. = 181–183 °C; ^{1}H-NMR (500 MHz, DMSO-d_6): δ = 2.40 (s, 3H), 6.97 (s, 2H), 7.25 (s, 1H), 7.37 (d, J = 7.5 Hz, 2H), 7.47–7.50 (m, 3H), 7.59 (d, J = 7.5 Hz, 2H), 8.11–8.13 (m, 2H) ppm. ^{13}C-NMR (125 MHz, DMSO-d_6): δ = 20.8, 86.5, 109.1, 117.1, 127.2, 128.2, 128.6, 129.3, 130.0, 134.1, 137.6, 139.3, 154.8, 158.5, 160.9 ppm.

2-Amino-7,7-dimethyl-5-oxo-4-phenyl-5,6,7,8-tetrahydro-4*H*-chromene-3-carbonitrile[66] (16b). Yield 50%, the pale yellow powder. R_f = 0.52 (n-hexane–EtOAc = 5 : 5); Mp. = 233–234 °C; ^{1}H-NMR (500 MHz, DMSO-d_6): δ = 0.96 (s, 3H), 1.04 (s, 3H), 2.11 (d, J = 16.0 Hz, 1H), 2.26 (d, J = 16.0 Hz, 1H), 2.48–2.58 (m, 2H), 4.17 (s, 1H), 7.00 (s, 2H), 7.14 (d, J = 7.5 Hz, 2H), 7.18 (t, J = 7.5 Hz, 1H), 7.28 (t, J = 7.5 Hz, 2H) ppm. ^{13}C-NMR (125 MHz, DMSO-d_6): δ = 26.8, 28.4, 31.8, 35.6, 50.0, 58.3, 112.7, 119.7, 126.5, 127.1, 128.3, 144.7, 158.5, 162.5, 195.6 ppm.

2-Amino-4-(4-methoxyphenyl)-7,7-dimethyl-5-oxo-5,6,7,8-tetrahydro-4*H*-chromene-3-carbonitrile[66] (17b). Yield 14%, the pale yellow powder. R_f = 0.48 (n-hexane–EtOAc = 5 : 5); Mp. = 200–202 °C; ^{1}H-NMR (500 MHz, DMSO-d_6): δ = 0.94 (s, 3H), 1.03 (s, 3H), 2.08 (d, J = 16.0 Hz, 1H), 2.24 (d, J = 16.0 Hz, 1H), 2.45–

2.45 (m, 2H), 3,71 (s, 3H), 4.12 (s, 1H), 6.84 (d, J = 8.5 Hz, 2H), 6.95 (s, 2H), 7.05 (d, J = 8.5 Hz, 2H) ppm. ^{13}C-NMR (125 MHz, DMSO-d_6): δ = 26.8, 28.4, 31.8, 34.7, 50.0, 55.0, 58.6, 113.0, 113.7, 119.8, 128.2, 136.8, 157.9, 158.4, 162.1, 195.0 ppm.

2-Amino-4-(4-fluorophenyl)-7,7-dimethyl-5-oxo-5,6,7,8-tetrahydro-4*H*-chromene-3-carbonitrile[66] (18b). Yield 75%, the pale yellow powder. R_f = 0.48 (*n*-hexane–EtOAc = 5 : 5); Mp. = 184–185 °C; ^{1}H-NMR (500 MHz, DMSO-d_6): δ = 0.94 (s, 3H), 1.03 (s, 3H), 2.11 (d, J = 16.0 Hz, 1H), 2.25 (d, J = 16.0 Hz, 1H), 2.47–2.54 (m, 2H), 3,71 (s, 3H), 4.20 (s, 1H), 7.03 (s, 2H), 7.10 (t, J = 8.5 Hz, 2H), 7.16–7.19 (m, 2H) ppm. ^{13}C-NMR (125 MHz, DMSO-d_6): δ = 26.8, 28.3, 31.8, 34.9, 50.0, 58.1, 112.6, 115.0 (d, J = 21.3 Hz), 119.6, 129.0 (d, J = 7.5 Hz), 140.9 (d, J = 2.5 Hz), 158.5, 160.9 (d, J = 241.3 Hz), 162.5, 195.7 ppm.

2-Amino-4-(2-chlorophenyl)-7,7-dimethyl-5-oxo-5,6,7,8-tetrahydro-4*H*-chromene-3-carbonitrile[66] (19b). Yield 7%, the pale yellow powder. R_f = 0.51 (*n*-hexane–EtOAc = 5 : 5); Mp. = 213–215 °C; ^{1}H-NMR (500 MHz, DMSO-d_6): δ = 0.98 (s, 3H), 1.04 (s, 3H), 2.08 (d, J = 16.0 Hz, 1H), 2.25 (d, J = 16.0 Hz, 1H), 2.47–2.57 (m, 2H), 4.69 (s, 1H), 7.03 (s, 2H), 7.16–7.22 (m, 2H), 7.27 (t, J = 7.0 Hz, 1H), 7.36 (d, J = 8.0 Hz, 1H) ppm. ^{13}C-NMR (125 MHz, DMSO-d_6): δ = 26.9, 28.4, 31.8, 32.8, 49.9, 56.8, 111.8, 119.2, 127.4, 128.2, 129.4, 130.0, 132.1, 141.6, 158.7, 163.1, 195.5 ppm.

2-Amino-4-(2-fluorophenyl)-7,7-dimethyl-5-oxo-5,6,7,8-tetrahydro-4*H*-chromene-3-carbonitrile (20b). Yield 42%, the yellow powder. R_f = 0.52 (*n*-hexane–EtOAc = 5 : 5); Mp. = 237–239 °C; ^{1}H-NMR (500 MHz, DMSO-d_6): δ = 0.96 (s, 3H), 1.04 (s, 3H), 2.08 (d, J = 16.0 Hz, 1H), 2.27 (d, J = 16.0 Hz, 1H), 2.45–2.57 (m, 2H), 4.45 (s, 1H), 7.03 (s, 2H), 7.09–7.13 (m, 2H), 7.17 (t, J = 7.5 Hz, 1H), 7.21–7.25 (m, 1H) ppm. ^{13}C-NMR (125 MHz, DMSO-d_6): δ = 26.6, 28.5, 29.8, 31.8, 49.9, 56.7, 111.4, 115.4 (d, J = 21.3 Hz), 119,5, 124,4 (d, J = 2.5 Hz), 128.6 (d, J = 7.5 Hz), 129.7 (d, J = 3.8 Hz), 131.2 (d, J = 12.5 Hz), 158.8, 159.9 (d, J = 245.0 Hz), 163.1, 195.6 ppm.

2-Amino-4-(4-bromophenyl)-7,7-dimethyl-5-oxo-5,6,7,8-tetrahydro-4*H*-chromene-3-carbonitrile[66] (21b). Yield 8%, the pale yellow powder. R_f = 0.53 (*n*-hexane–EtOAc = 5 : 5); Mp. = 232–234 °C; ^{1}H-NMR (500 MHz, DMSO-d_6): δ = 1.00 (s, 6H), 2.33 (s, 2H), 2.83 (s, 2H), 7.15 (d, J = 8.5 Hz, 2H), 7.60 (d, J = 8.5 Hz, 2H), 7.73 (s, 2H) ppm. ^{13}C-NMR (125 MHz, DMSO-d_6): δ = 27.7, 31.6, 46.9, 52.4, 90.8, 115.3, 115.6, 121.3, 129.5, 130.8, 137.3, 155.6, 160.3, 168.1, 194.0 ppm.

2-Amino-7,7-dimethyl-5-oxo-4-(*p*-tolyl)-5,6,7,8-tetrahydro-4*H*-chromene-3-carbonitrile[66] (22b). Yield 6%, the pale yellow powder. R_f = 0.57 (*n*-hexane–EtOAc = 5 : 5); Mp. = 200–202 °C; ^{1}H-NMR (500 MHz, DMSO-d_6): δ = 1.00 (s, 6H), 2.32 (s, 2H), 2.36 (s, 3H), 2.83 (s, 2H), 7.05 (d, J = 8.0 Hz, 2H), 7.20 (d, J = 8.0 Hz, 2H), 7.64 (s, 2H) ppm. ^{13}C-NMR (125 MHz, DMSO-d_6): δ = 20.9, 27.7, 31.6, 47.0, 52.6, 91.1, 115.5, 116.0, 127.3, 128.4, 135.0, 137.1, 156.9, 160.3, 167.9, 193.9 ppm.

2-Amino-4-(furan-2-yl)-7,7-dimethyl-5-oxo-5,6,7,8-tetrahydro-4*H*-chromene-3-carbonitrile (23b). Yield 28%, the pale yellow powder. R_f = 0.49 (*n*-hexane–EtOAc = 5 : 5); Mp. = 218–220 °C; ^{1}H-NMR (500 MHz, DMSO-d_6): δ = 0.98 (s, 3H), 1.04 (s, 3H), 2.17 (d, J = 16.0 Hz, 1H), 2.29 (d, J = 16.0 Hz, 1H), 2.43–2.54 (m, 2H), 4.32 (s, 1H), 6.05 (d, J = 3.0 Hz, 1H), 6.32 (dd, J = 2.0 Hz, 3.0 Hz, 1H), 7.48 (d, J = 2.0 Hz, 1H) ppm. ^{13}C-NMR (125 MHz, DMSO-d_6): δ = 26.6, 28.4, 29.0, 31.8, 49.9, 55.4, 105.1, 110.4, 110.5, 119.6, 141.8, 155.7, 159.3, 163.6, 195.4 ppm.

The procedural steps involved in the recycling of ETG-acetamide

After the conclusion of the reaction, the solid catalyst was isolated and subjected to a washing procedure including distilled water (5 × 3 mL) and acetone (5 × 3 mL). This washing process was monitored through the use of TLC. Subsequently, the catalyst was dried at ambient temperature in preparation for the subsequent reaction. The catalyst was further used through the optimal conditions and the recycling process was the same. The data was collected until 3 recycle times.

Conclusions

This research presents a pioneering and environmentally conscious approach for synthesizing pyridine and chromene derivatives. The proposed methodology encompasses a unified, multi-component synthesis wherein arylaldehydes, cyclohexanone/dimedone, malononitrile, and ammonium acetate are combined in a single reaction vessel. This reaction is facilitated by the implementation of ETG-acetamide, which serves as both a green catalyst and solvent. This methodology presents numerous benefits, such as the utilization of an environmentally friendly ETG instead of hazardous organic solvents or catalysts (or both) achieving considerable product yields, employing a straightforward work-up protocol, and enabling the recyclability.

Author contributions

Phat Ngoc Nguyen: investigation, methodology, resources, formal analysis, validation, data curation writing – original draft; Linh Ho Thuy Nguyen: methodology, resources, formal analysis, Tan Le Hoang Doan: resources, formal analysis, writing – review & editing, Phuong Hoang Tran: methodology, resources, formal analysis, writing – review & editing; Hai Truong Nguyen: methodology, resources, formal analysis, validation, data curation, writing – review & editing, supervision.

Conflicts of interest

There are no conflicts to declare.

Acknowledgements

This research is funded by Vietnam National University, Ho Chi Minh City (VNU-HCM) under grant number C2023-18-09.

Notes and references

1 K. N. Ganesh, D. Zhang, S. J. Miller, K. Rossen, P. J. Chirik, M. C. Kozlowski, J. B. Zimmerman, B. W. Brooks, P. E. Savage, D. T. Allen and A. M. Voutchkova-Kostal, *Environ. Sci. Technol. Lett.*, 2021, **8**, 487–491.
2 D. Yu, Z. Xue and T. Mu, *Cell Rep. Phys. Sci.*, 2022, **3**, 100809.

3 S. Zangade and P. Patil, *Curr. Org. Chem.*, 2019, **23**, 2295–2318.
4 M. Sepahvand, F. Buazar and M. H. Sayahi, *Appl. Organomet. Chem.*, 2020, **34**, e6000.
5 M. H. Zainal-Abidin, M. Hayyan, A. Hayyan and N. S. Jayakumar, *Anal. Chim. Acta*, 2017, **979**, 1–23.
6 M. Espino, M. de los Ángeles Fernández, F. J. Gomez and M. F. Silva, *TrAC, Trends Anal. Chem.*, 2016, **76**, 126–136.
7 S. C. Cunha and J. O. Fernandes, *TrAC, Trends Anal. Chem.*, 2018, **105**, 225–239.
8 S. Massayev and K. M. Lee, *J. Cleaner Prod.*, 2022, **360**, 132239.
9 A. M. Ramezani, R. Ahmadi and Y. Yamini, *TrAC, Trends Anal. Chem.*, 2022, **149**, 116566.
10 L. B. Santos, R. S. Assis, J. A. Barreto, M. A. Bezerra, C. G. Novaes and V. A. Lemos, *TrAC, Trends Anal. Chem.*, 2022, **146**, 116478.
11 M. Shaibuna, L. V. Theresa and K. Sreekumar, *Soft Matter*, 2022, **18**, 2695–2721.
12 J. Wang, S. Zhang, Z. Ma and L. Yan, *Green Chem. Eng.*, 2021, **2**, 359–367.
13 Y. Liang, K. Wang, J. Li, H. Wang, X. Q. Xie, Y. Cui, Y. Zhang, M. Wang and C. S. Liu, *Adv. Funct. Mater.*, 2021, **31**, 2104963.
14 X. Hou, T. P. Pollard, X. He, L. Du, X. Ju, W. Zhao, M. Li, J. Wang, E. Paillard and H. Lin, *Adv. Energy Mater.*, 2022, **12**, 2200401.
15 B. Joos, T. Vranken, W. Marchal, M. Safari, M. K. Van Bael and A. T. Hardy, *Chem. Mater.*, 2018, **30**, 655–662.
16 H. Sereshti, Z. Mohammadi, S. Soltani and M. Taghizadeh, *Talanta*, 2023, 124801.
17 N. Bhardwaj, A. Pathania and P. Kumar, *Curr. Tradit. Med.*, 2021, **7**, 5–27.
18 S. Bera, A. Biswas and R. Samanta, *Chem. Rec.*, 2021, **21**, 3411–3428.
19 R. J. Obaid, E. U. Mughal, N. Naeem, M. M. Al-Rooqi, A. Sadiq, R. S. Jassas, Z. Moussa and S. A. Ahmed, *Process Biochem.*, 2022, **120**, 250–259.
20 R. Sreedevi, S. Saranya, K. Rohit and G. Anilkumar, *Adv. Synth. Catal.*, 2019, **361**, 2236–2249.
21 K. Ilina and M. Henary, *Chem.–Eur. J.*, 2021, **27**, 4230–4248.
22 B. S. Arslan, S. N. Ülüş, M. Gezgin, B. Arkan, E. Güzel, D. Avcı, M. Nebioğlu and İ. Şişman, *Opt. Mater.*, 2020, **106**, 109974.
23 P. Panda and S. Chakroborty, *ChemistrySelect*, 2020, **5**, 10187–10199.
24 P. Ghasemi, M. Yarie, M. A. Zolfigol, A. A. Taherpour and M. Torabi, *ACS Omega*, 2020, **5**, 3207–3217.
25 M. V. De Souza, K. C. Pais, C. R. Kaiser, M. A. Peralta, M. D. L. Ferreira and M. C. Lourenço, *Bioorg. Med. Chem.*, 2009, **17**, 1474–1480.
26 C. dos Santos Chagas, F. L. Fonseca and I. A. Bagatin, *Mater. Sci. Eng., C*, 2019, **98**, 1043–1052.
27 A. A. Cheriyan, L. Thomas and A. Singhal, *Chem. Biol. Lett.*, 2022, **9**, 318.
28 S. Rajendran, K. Sivalingam, R. P. Karnam Jayarampillai, W. L. Wang and C. O. Salas, *Chem. Biol. Drug Des.*, 2022, **100**, 1042–1085.
29 Z. N. Siddiqui, N. Ahmed, F. Farooq and K. Khan, *Tetrahedron Lett.*, 2013, **54**, 3599–3604.
30 M. A. Ghasemzadeh and J. Safaei-Ghomi, *J. Chem. Res.*, 2014, **38**, 313–316.
31 A. Maleki and S. Azadegan, *Inorg. Nano-Met.*, 2017, **47**, 917–924.
32 M. Mashhadinezhad, M. Mamaghani, M. Rassa and F. Shirini, *ChemistrySelect*, 2019, **4**, 4920–4932.
33 A. Purkhosrowa, S. M. Haghighib, A. Khalafi-Nezhadb and S. Oftadehgana, *Iran J. Org. Chem.*, 2022, **14**, 3255–3263.
34 A. Singh, K. U. Saumya, M. Joshi, N. Kaur, N. Garg and N. Singh, *New J. Chem.*, 2023, **47**, 8589–8601.
35 Z. Arzehgar, V. Azizkhani, S. Sajjadifar and M. Fekri, *Chem. Methodol.*, 2019, **3**, 251–260.
36 J. Dadashi, M. A. Ghasemzadeh and M. H. Abdollahi-Basir, *Polycyclic Aromat. Compd.*, 2023, **43**, 7266–7278.
37 K. Azizi, M. Karimi, H. R. Shaterian and A. Heydari, *RSC Adv.*, 2014, **4**, 42220–42225.
38 M. Ali Ghasemzadeh, Z. Elyasi, M. Azimi-Nasrabad and B. Mirhosseini-Eshkevari, *J. Comb. Chem. High Throughput Screening*, 2017, **20**, 64–76.
39 Y. Liu, S. Cao, Z. Liu, D. Wu, M. Luo and Z. Chen, *Chemosphere*, 2023, **323**, 138276.
40 Y. Li, Y. Li, C. Cao, H. Li, X. Fan, X. Xu and M. Zhu, *J. Mol. Liq.*, 2022, **365**, 120162.
41 N. Mehrabi, U. F. Abdul Haq, M. T. Reza and N. Aich, *J. Environ. Chem. Eng.*, 2020, **8**, 104222.
42 Y. Wang, J. Wang, Z. Ma and L. Yan, *ACS Appl. Mater. Interfaces*, 2021, **13**, 54409–54416.
43 X.-J. Zha, S.-T. Zhang, J.-H. Pu, X. Zhao, K. Ke, R.-Y. Bao, L. Bai, Z.-Y. Liu, M.-B. Yang and W. Yang, *ACS Appl. Mater. Interfaces*, 2020, **12**, 23514–23522.
44 S. Asadbegi, M. A. Bodaghifard and A. Mobinikhaledi, *Res. Chem. Intermed.*, 2020, **46**, 1629–1643.
45 M. Edrisi and N. Azizi, *J. Iran. Chem. Soc.*, 2020, **17**, 901–910.
46 N. Mollakarimi Dastjerdi and M. Ghanbari, *Green Chem. Lett. Rev.*, 2020, **13**, 192–205.
47 S. S. Mansoor, K. Aswin, K. Logaiya, P. N. Sudhan and S. Malik, *Res. Chem. Intermed.*, 2014, **40**, 871–885.
48 J. Safari, S. H. Banitaba and S. D. Khalili, *Ultrason. Sonochem.*, 2012, **19**, 1061–1069.
49 M. Zadpour and F. K. Behbahani, *Monatsh. Chem.*, 2015, **146**, 1865–1869.
50 Z. Hosseinzadeh, A. Ramazani, H. Ahankar, K. Ślepokura and T. Lis, *Silicon*, 2019, **11**, 2169–2176.
51 M. A. Zolfigol, M. Kiafar, M. Yarie, A. A. Taherpour and M. Saeidi-Rad, *RSC Adv.*, 2016, **6**, 50100–50111.
52 A. Moshtaghi Zonouz, S. Okhravi and D. Moghani, *Monatsh. Chem.*, 2016, **147**, 1819–1824.
53 D. Fang, H. B. Zhang and Z. L. Liu, *J. Heterocycl. Chem.*, 2010, **47**, 63–67.
54 J. Safaei-Ghomi, R. Aghagoli and H. Shahbazi-Alavi, *Z. Naturforsch. B*, 2018, **73**, 269–274.
55 A. Khazaei, H. A. A. Nik, A. R. Moosavi-Zare and H. Afshar-Hezarkhani, *Z. Naturforsch. B*, 2018, **73**, 707–712.
56 N. Azizi, S. Dezfooli, M. Khajeh and M. M. Hashemi, *J. Mol. Liq.*, 2013, **186**, 76–80.

57 D. Patil, D. Chandam, A. Mulik, S. Jagdale, P. Patil and M. Deshmukh, *J. Saudi Chem. Soc.*, 2017, **21**, S329–S338.
58 A. Barzkar and A. S. Beni, *RSC Adv.*, 2020, **10**, 41703–41712.
59 T. Akbarpoor, A. Khazaei, J. Y. Seyf, N. Sarmasti and M. M. Gilan, *Res. Chem. Intermed.*, 2020, **46**, 1539–1554.
60 S. Khaksar and M. Yaghoobi, *J. Fluorine Chem.*, 2012, **142**, 41–44.
61 Y. Wan, R. Yuan, F.-R. Zhang, L.-L. Pang, R. Ma, C.-H. Yue, W. Lin, W. Yin, R.-C. Bo and H. Wu, *Synth. Commun.*, 2011, **41**, 2997–3015.
62 R. K. A. M. Ghamari, *J. Braz. Chem. Soc.*, 2016, **27**, 759–768.
63 D. Khalili, *Tetrahedron Lett.*, 2016, **57**, 1721–1723.
64 Y. M. Elkholy and M. A. Morsy, *Molecules*, 2006, **11**, 890–903.
65 S. Asadbegi, M. A. Bodaghifard and A. Mobinikhaledi, *Res. Chem. Intermed.*, 2020, **46**, 1629–1643.
66 M. A. Nasseri and S. M. Sadeghzadeh, *J. Iran. Chem. Soc.*, 2013, **10**, 1047–1056.